



Cite this: *J. Mater. Chem. B*, 2016, 4, 2553

Surface functionalized halloysite nanotubes decorated with silver nanoparticles for enzyme immobilization and biosensing†

Siva Kumar-Krishnan,^{*a} A. Hernandez-Rangel,^b Umapada Pal,^c O. Ceballos-Sanchez,^d F. J. Flores-Ruiz,^e E. Prokhorov,^b O. Arias de Fuentes,^{bf} Rodrigo Esparza^a and M. Meyyappan^g

Improving enzyme immobilization with high loading capacity and achieving direct electron transfer (DET) between the enzyme and the electrode surface is key to designing highly sensitive enzymatic electrochemical biosensors. Herein, we report a novel approach based on the selective modification of the outer surface of halloysite nanotubes (HNTs) that supports silver nanoparticles (AgNPs) to obtain a hybrid nanocomposite. AgNPs of about 10 nm average size could be uniformly supported on silane-modified HNTs through *in situ* reduction of Ag⁺ ions. The resultant nanocomposite shows an excellent support capability for the effective immobilization and electrical wiring of redox enzyme glucose oxidase (GOx). The GOx immobilized HNT/AgNPs were deposited on the glassy carbon electrode (GCE) and utilized for the bioelectrocatalyzed electrochemical detection of glucose. The GOx modified composite electrodes show glucose sensitivity as high as 5.1 $\mu\text{A mM}^{-1} \text{cm}^{-2}$, which is higher than for the electrodes prepared without surface functionalization.

Received 7th January 2016,
Accepted 9th March 2016

DOI: 10.1039/c6tb00051g

www.rsc.org/MaterialsB

Introduction

The enzyme immobilization process has attracted significant research interest in recent years due to its diverse applications including in biocatalysts, biofuel cells, biosensing, biorecognition and drug delivery.^{1–3} In particular, the integration of enzymes onto nanoparticle (NP) surfaces to improve the direct electron transfer (DET) between immobilized enzymes and electrode surface remains a challenge for designing highly sensitive enzymatic biosensors^{4,5} and biofuel cells.⁶ Several approaches have been proposed to overcome the challenges associated with the effective immobilization and electrical wiring of redox-active cofactors. For example,

flavin adenine dinucleotide (FAD) has been contacted with the electrode surface in order to improve the DET process.^{5,7–10} Enzyme immobilization onto a given solid matrix is the key factor that significantly affects the biosensor performance. Low operational stability, poor preservation of biocatalytic functions, and high cost of fabrication are the principal problems associated with designing efficient biosensors. The loss in the biocatalytic activity of surface immobilized enzymes is mainly attributed to a change in the structure of the enzyme from its native form to an unfolded structure.¹¹ Considerable attempts have been made to develop ideal matrix materials to overcome these problems by exploring a wide range of supports including polymers,¹² conducting hydrogels,¹³ block copolymers,¹⁴ polymeric brushes and microcapsules,^{8,15} mesoporous silica,¹⁶ DNA scaffolds,¹⁰ metal organic frameworks (MOFs),^{17,18} graphene oxide (GO)¹⁹ and carbon nanotubes (CNTs)²⁰ all of them aiming for the effective immobilization of redox enzymes without losing their activity and improvement of the DET process between the FAD cofactor in GOx and the electrode surface. However, the high cost of these materials, difficulties in large-scale preparation, poor stability and biocompatibility issues limit their practical applications and commercial success.²¹ Among the wide range of materials explored, halloysite nanotubes (HNTs) occupy a prominent place due to their low-cost and hollow tubular structure. Apart from high surface area due to the tubular structure, the low material density makes them ideal matrices for decoration with a wide range of inorganic nanoparticles, *i.e.* for the development of

^a Centro de Física Aplicada y Tecnología Avanzada, Universidad Nacional Autónoma de México, Boulevard Juriquilla 3001, Santiago de Querétaro, Qro., 76230, Mexico. E-mail: skumar@fata.unam.mx; Tel: +52-1-5556234173

^b Cinvestav-Querétaro, Querétaro, Qro., 76230, Mexico

^c Instituto de Física, Benemérita Universidad Autónoma de Puebla, Apdo. Postal J-48, Puebla 72570, Mexico

^d Cátedras Conacyt at Facultad de Ingeniería Civil, Departamento de Ecomateriales y Energía, Universidad Autónoma de Nuevo León (UANL), Ciudad Universitaria, San Nicolás de los Garza, Nuevo León C.P. 64451, Mexico

^e Centro de Nanociencias y Nanotecnología-UNAM, Ensenada, BC, 22860, Mexico

^f Instituto de Ciencia y Tecnología de Materiales, Universidad de La Habana, 10400, Cuba

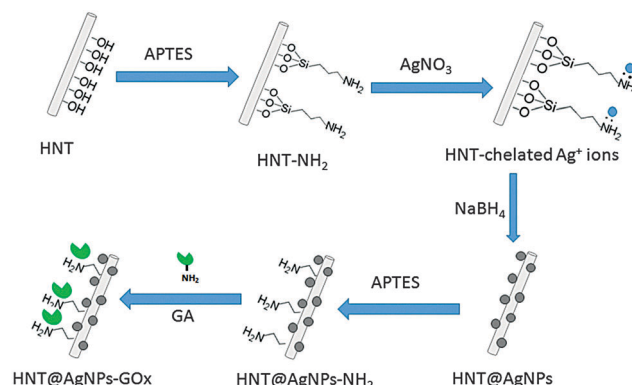
^g NASA Ames Research Center, Moffett Field, CA 94035, USA

† Electronic supplementary information (ESI) available: EDS mapping, FT-IR and comparison of CVs of different modified electrodes. See DOI: 10.1039/c6tb00051g

hybrid organic/inorganic composites.²² Besides, distinct structural features such as environmental friendliness, biocompatibility and hollow tubular structure with an inner diameter of 5–20 nm and a pore size of 0.3–2 nm, HNTs have enabled novel support for the effective immobilization of biomolecules.²³ Enzymes can be immobilized with higher loading without compromising their activities.²⁴ In addition, the curved surface of the support can suppress the interaction between the adjacent enzymes and allow multipoint bond formation, reducing the possibility of enzyme aggregation on the surface of the support. As a result, the structural integrity and biocatalytic activity of the enzyme can be significantly regulated.^{25,26}

The rapid advances in the synthesis of organic/inorganic hybrid composite materials such as metal nanoparticles in the organic matrix have attracted great attention due to their enhanced catalytic, photocatalytic and other functionalities.²⁷ In particular, rational incorporation of metallic nanoparticles into HNTs holds significant potential for catalytic^{22,28} and biosensing applications.²⁹ Enhanced amperometric glucose sensing and microbial fuel cell performance by metal nanoparticle mediated DET have been demonstrated recently.^{7,30,31} The metal NPs attached to the electrode surface act as an electrocatalyst through direct electrical wiring with the deeply buried FAD co-factor unit in GOx.³² Among the metal nanoparticles, silver nanoparticles (AgNPs) have received special attention for such applications due to their high electrical conductivity, excellent biocatalytic activity, and low-cost. On the other hand, the immobilization of GOx enzymes onto a solid matrix through direct physical adsorption,²⁰ covalent anchoring³³ or non-covalent π - π functionalization³⁴ can protect the enzymes from degradation. However, the direct physical adsorption of enzymes over a solid matrix often leads to partial deactivation of their biocatalytic functions and consequently DET is not observed.³⁵ Similarly, the immobilization of enzymes over 3D redox polymer matrices significantly impacts the charge-transfer efficiency. Modification of the NP surface with functional groups and immobilization of enzymes through covalent bonding was found to be an effective pathway to overcome the problems associated with non-specific binding, charge transfer efficiency, and stability of the enzymes. As a result, highly improved biocatalytic activities and improved charge transfer between the FAD center in GOx enzymes and the electrode surface is observed.^{2,14,36,37}

As a step forward to overcome this problem, we utilized silane-modified HNTs in this work to prepare HNT/AgNP hybrid nanocomposites, and implemented for the effective immobilization and electrical wiring of glucose oxidase (GOx) enzymes. Excellent dispersion of AgNPs of significantly smaller particle size (approx. 10 nm) over HNTs was achieved through *in situ* chemical reduction by sodium borohydride (NaBH₄) utilizing the interaction between the nanoparticles and the NH₂ groups over HNT surfaces. In fact, the effective incorporation of metal nanoparticles into HNT surfaces on a large-scale through surface modification by APTES has been demonstrated by several research groups.^{22,28,38} Recently, Cong Chao and co-workers showed that dopamine functionalized HNTs can be used for the immobilization of lactase enzymes over their external surfaces with



Scheme 1 Schematic illustration of the selective modification of the HNTs and subsequent grafting of AgNPs and site-specific covalent immobilization of the GOx enzymes.

enzyme-loading efficiency as high as 168.8 mg g⁻¹, while retaining more than 90% of activity after 30 days of storage.³⁹ The significant improvement in enzyme loading and the biocatalytic activity of the structures was due to the formation of covalent bonds between immobilized GOx and the amine modified HNT surfaces. However, the relatively poor electronic conductivity and the low electrocatalytic activity of HNTs significantly limit their practical applications as biosensors.

Herein, we report a versatile strategy to modify the external surface of HNTs using APTES for the growth and homogeneous attachment of AgNPs. APTES is also used to functionalize the HNT/AgNP surface to introduce NH₂ groups for site-specific covalent immobilization of GOx enzyme (Scheme 1). The good electrical contact between GOx and the HNT/AgNP composite surface is expected to facilitate electrical wiring between the FAD co-factor unit and the electrode surface.⁸ Electrochemical detection of glucose based on the covalently immobilized HNT/AgNPs/GOx modified electrodes was performed and compared with unmodified HNT/AgNPs/GOx. The GOx modified HNT/AgNP electrodes demonstrate high sensitivity for glucose detection with high stability.

Experimental

Materials

HNTs, silver nitrate (AgNO₃, ≥99%), sodium borohydride (NaBH₄, ≥99.99%), nitric acid, (3-aminopropyl) triethoxysilane (APTES, 99%), glucose oxidase (GOx, from *Aspergillus niger*; 15–50 K units per g), and D-glucose (≥99.5%) were purchased from Sigma-Aldrich. Acetic acid (glacial, 99–100%) was purchased from Merck. All other reagents were of analytical grade and used as received. Ultrapure deionized (DI) water (18 MΩ cm) was used for all electrochemical experiments.

Preparation of aminosilane modified HNTs

The aminosilane modified HNTs were prepared by a previously reported protocol³⁶ with some modifications. First, a 95 mL ethanol–water mixture (95 : 5, v/v) containing 5 g of HNTs was taken in a three-necked round bottom flask fitted with a condenser.

The pH of the solution mixture was adjusted to 4 by adding dilute acetic acid (1%) under magnetic stirring for 15 min. Then 5 g of APTES solution was added drop-wise to the mixture. The reaction solution was refluxed at 120 °C for 12 h. After cooling to room temperature, the precipitated HNTs were washed twice with an ethanol–water mixture (95:5, v/v). The surface functionalized HNTs were dried at 100 °C for 5 h and used for further synthetic work.

Synthesis of HNT/AgNP hybrid composites

HNT/AgNP composites were prepared using AgNO₃ as a silver precursor. Silver ions were *in situ* reduced to silver nanoparticles, which were subsequently stabilized on the NH₂ modified HNTs as depicted in Scheme 1. In a typical synthesis process, 0.5 g of surface modified HNTs was added to 10 mL of DI water and magnetically stirred to disperse homogeneously. After that, 1 mL of AgNO₃ solution (0.2 M) was slowly added to the solution mixture and magnetically stirred for 30 min to obtain HNTs/Ag⁺ ion mixtures and then reduced using 2 mL of freshly prepared aqueous NaBH₄ (0.1 M) solution. The color of the reaction mixture turned white to dark yellow, suggesting the formation of AgNPs over HNT surfaces. The resultant product was washed several times with DI water to remove unreacted Ag⁺ ions (if any) and byproducts.

Surface functionalization and covalent immobilization of GOx on HNT/AgNP hybrids

Glucose oxidase (GOx) redox enzymes were used for the immobilization process due to its well-studied application in glucose sensing. In a typical immobilization process, 0.5 g of as-prepared HNT/AgNP composite was surface functionalized again with the APTES using the same protocol as the functionalization of HNTs. The product was washed with DI water to remove excess NH₂ groups. After removing the excess NH₂ groups, the NH₂ terminated HNT/AgNP composite was dispersed in 5 mL of 0.1M phosphate buffer (PBS, pH 7.4) containing 1 mL of glutaraldehyde (GA, 50%) under mechanical stirring for 2 h. The composite was then separated by centrifugation and redispersed in PBS (0.1 M). This activated composite was then added to a PBS solution (0.1 M) containing GOx (20 mg mL⁻¹) and incubated overnight for the covalent immobilization of GOx (HNT/AgNPs/GOx). The product was rinsed again with DI water and separated by centrifugation at 6000 rpm to remove unbound GOx. The immobilized HNT/AgNPs/GOx was then stored at 4 °C.

Preparation of HNT/AgNPs/GOx hybrid electrodes

Homemade glassy carbon electrodes (GCEs) of about 3 mm diameter were carefully polished with 1.0 and 0.3 μm alumina powders to obtain a mirror-like surface and washed with an water/ethanol mixture for 15 min under sonication. Then, the cleaned electrodes were checked in 1 M KCl solution containing 2 mM K₃Fe (CN)₆ at a scan rate of 50 mV s⁻¹ for reversible electron transfer.⁴⁰ After that, 30 μL of immobilized HNT/AgNPs/GOx dispersion was drop-casted over pre-treated GCE electrodes, allowed to dry at room temperature, and stored at 4 °C.

Material characterization

The morphology of the HNT and HNT/AgNP samples were analyzed using a JEOL JEM-1010 transmission electron microscope (TEM) operating at 80 kV. The size distribution and average size of the AgNPs were measured from the TEM images using imageJ software. Elemental distribution in the nanostructures was monitored through energy dispersive spectroscopy (EDS) mapping in a Hitachi SU 8020 scanning transmission electron microscope (STEM). An Agilent 8453 UV-vis spectrophotometer was used to study the optical properties of the nanostructures at room temperature. X-ray diffraction spectra of the samples were acquired using CuKα radiation ($\lambda = 1.5406 \text{ \AA}$) of a Rigaku ULTIMA IV diffractometer. A Perkin Elmer spectrometer with an ATR accessory was used to record the Fourier transform infrared (FT-IR) spectra of the samples in the 4000–650 cm⁻¹ spectral range. For the analysis of the composition and chemical states of the elements, high-resolution X-ray photoelectron spectra (XPS) of the samples were collected in a non-monochromatic Al Kα (1486.7 eV) X-ray source and a hemispherical electron analyzer with seven channeltrons (model XPS110). All the recorded XPS spectra were corrected utilizing C 1s line at 284.8 eV. The texture properties of the samples were evaluated through their N₂ adsorption–desorption isotherms at 77 K utilizing a Belsorp Mini-II sorptometer (BEL, Japan) after degassing at 180 °C for 8 h. Atomic microscopy (AFM) images of the samples were acquired using a commercial SPM-AFM system (Bruker/Veeco/Digital Instruments Nanoscope IV Dimension 3100 system) at room temperature by drop-casting about 10 μL of HNT/AgNPs/GOx stock solution over silicon substrates and subsequent drying. The topographic images were obtained using a diamond-coated silicon AFM probe (Budget Sensors model ContDLC) with a nominal length of 300 μm, in tapping mode at a resonance frequency of 13 kHz. The images were analyzed using Gwyddion software.

Electrochemical measurements

All the electrochemical experiments were performed in a standard three-electrode (VoltaLab 40 PGZ 301) electrochemical cell. Platinum foil was used as the auxiliary electrode and a saturated calomel electrode (SCE) as the reference one. The working electrodes were homemade modified glassy carbon electrodes. The glucose sensing performance of the modified electrodes was tested through cyclic voltammetry (CV) measurements. The CV characteristics of the samples were recorded in O₂-saturated 0.1M PBS (pH 7.4) solution with the addition of glucose at different concentrations.

Results and discussion

Structural characterization

The structure and morphology of HNTs and HNT/AgNPs were investigated by transmission electron microscopy (TEM) imaging. Fig. 1 shows the hollow tubular morphology and open ends of HNTs. The length of the HNTs varied in between 400 and 1000 nm and their diameter varied from 40 to 90 nm. Formation of AgNPs over the surface of APTES modified HNTs is clear in Fig. 1c and d. Ag nanoparticles of about 10 nm average size were homogeneously

grafted on the external surface of the HNTs through the surface terminated NH_2 groups. High-resolution TEM images of the surface-bound AgNPs also revealed their 10 nm average size. An estimated lattice spacing of 0.232 nm corresponds well to the (111) planes of Ag in a face centered cubic (fcc) structure (Fig. 1e and f).⁴¹ In addition to TEM analysis, high-angle annular dark field (HAADF) imaging and corresponding energy-dispersive X-ray spectroscopy (EDS) mapping were carried out to confirm the presence of AgNPs over the HNT surface. The HAADF images and EDS mappings of individual elements in HNT/AgNPs are presented in the ESI,[†] Fig. S1. A homogeneous distribution of AgNPs over HNTs can be clearly seen in the image of Fig. S1c (ESI[†]). The presence of AgNPs was further confirmed by the line scan EDS analysis across a single Ag nanoparticle over the HNT surface (ESI,[†] Fig. S1d). While the UV-vis optical absorption spectra of HNTs dispersed in DI water (Fig. 2a) revealed no absorption band in the 300–800 nm spectral range, the HNT/AgNPs sample dispersed in DI water revealed higher absorption with a sharp absorption band at around 403 nm, corresponding to the surface plasmon resonance (SPR) of small Ag particles.⁴²

X-ray diffraction (XRD) patterns of the functionalized HNT sample (Fig. 2b) revealed well defined diffraction peaks all corresponding to the HNT (JCPDS # 29-1487). Apart from these peaks, the XRD pattern of the HNT/AgNP composite sample revealed four new peaks at 2θ values of 38.0° , 44.28° , 64.25° and 77.48° , which correspond to the (111), (200), (220), and (311)

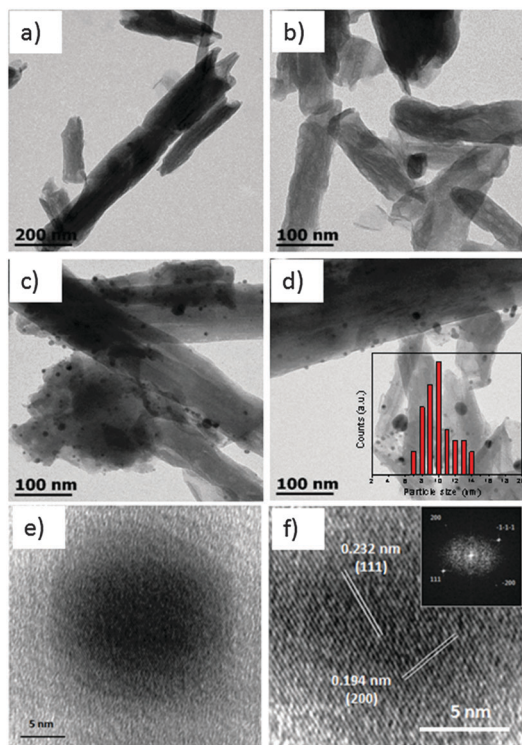


Fig. 1 Typical TEM images of (a and b) HNTs and (b and c) HNT/AgNPs. The inset in (d) shows the particle size distribution histogram of AgNPs over HNTs; (e and f) HRTEM images of the individual AgNPs grown over the HNT surface. The inset of (f) shows the corresponding FFT pattern.

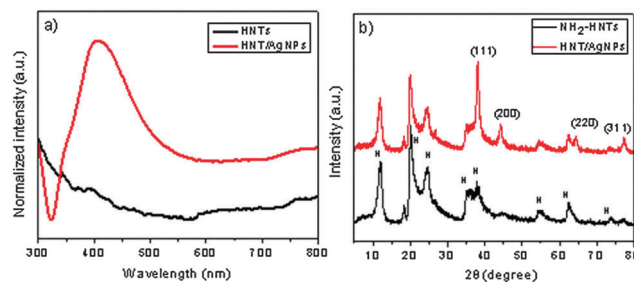


Fig. 2 (a) UV-vis spectra of the NH_2 -HNTs and HNT/AgNP composite; (b) XRD pattern of the NH_2 -modified HNT and HNT/AgNP hybrid composite.

planes of metallic silver in the fcc structure.³⁸ The absence of any other peak in the XRD pattern of the HNT/AgNP composite sample suggests that the modification by APTES does not affect the structure of HNTs.

The formation mechanism of the HNT/AgNP hybrid composite through selective surface modification of HNTs by APTES and subsequent *in situ* chemical reduction of silver ions by NaBH_4 are depicted in Scheme 1. The surface of HNTs was initially modified by the APTES to obtain amine functionalized HNTs (NH_2 -HNTs). The NH_2 terminated surfaces of HNTs pose high affinity for Ag^+ ions through ion chelation *via* nitrogen atoms.³⁸ Chelated Ag^+ ions were reduced to Ag atoms chemically by NaBH_4 to form Ag nanoparticle-grafted HNTs. Modification of the HNT surface usually leads to the formation of highly uniform metal particles at its surface with homogeneous dispersion.²²

Modification of the HNT surface by amino groups was studied by FT-IR spectroscopy. After surface modification by APTES, additional peaks appeared at around 3461 cm^{-1} , 2853 cm^{-1} and 922 cm^{-1} in the FT-IR spectrum of HNTs, which correspond to the N-H stretching vibrations, C-H asymmetric and symmetric vibrations, respectively, arising from APTES attached to the HNT surface (ESI,[†] Fig. S2).³⁸ The observed changes in the FT-IR spectra are consistent with previous reports.^{22,28} To confirm the selective surface functionalization and NH_2 -mediated incorporation of AgNPs on the HNTs further, X-ray photoelectron spectroscopy (XPS) was performed on the HNT/AgNP hybrid composite sample. Fig. 3a shows the XPS spectra of the Ag 3d and N 1s core levels for the HNT/AgNP sample. The Ag 3d region of silver is characterized by two peaks as a consequence of spin-orbital splitting that correspond to Ag $3d_{3/2}$ and Ag $3d_{5/2}$ core levels. The Ag 3d spectrum was deconvoluted into two doublets with a spin-orbit splitting at around 6.13 eV. The first doublet centered at lower binding energy (365.5 eV) was associated with metallic silver, while the less intense peaks in the second one centered at 367.9 eV was assigned to the unreduced Ag^+ ions that remain in the HNTs surface,^{42,43} indicating that almost 90% of the Ag^+ ions were reduced into AgNPs over the HNT surface. Effective surface functionalization of HNTs with amine groups was also monitored by the high-resolution XPS spectra of the N 1s core level as shown in Fig. 3b. The N 1s spectrum was fitted using two singlets associated with $-\text{NH}_2$ and $-\text{NH}-$ bonds at 401.15 and 403.22 eV, respectively. The presence of signals associated with NH_2 peaks further confirms the functionalization of HNTs with APTES.

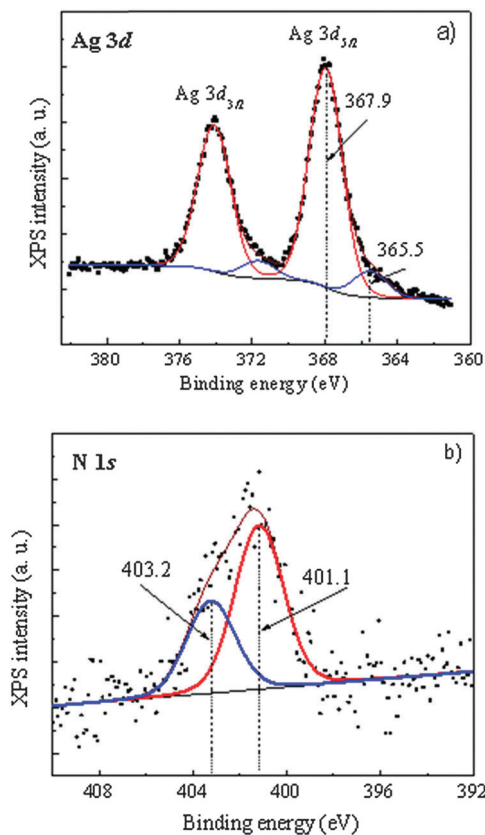


Fig. 3 High-resolution XPS spectra of (a) Ag 3d (b) N 1s core levels of the HNT/AgNP hybrid composite.

Nitrogen adsorption/desorption isotherms were recorded to calculate the specific surface area (SSA) of HNTs and HNT/AgNP hybrid structures (Fig. 4). Evolution of typical hysteresis loops with an abrupt increase in the adsorption at higher relative pressure (P/P_0) for the HNTs and HNT/AgNPs is indicative of their porous features. The SSA was calculated by the well-known Brunauer–Emmett–Teller (BET) method. Estimated SSAs for the HNT and HNT/AgNP samples were 120 and 128 $\text{m}^2 \text{g}^{-1}$, respectively. In comparison with the HNT, the surface modified HNT/AgNPs exhibit a higher SSA, which can be attributed to the presence of small AgNPs at the HNT surface, which is in good agreement with the previous report of a HNT supported with a TiO_2 composite.⁴⁴ The inset of Fig. 4 displays the pore-size distribution in the HNT/AgNP composite, which reveals narrow pore-size distribution with an average pore diameter of 14.5 nm. The observed average pore size is highly favorable for entrapping the GOx, which has dimensions of approximately 10 nm.^{10,33}

Analysis of enzyme immobilization on HNT/AgNP composites

The enzyme immobilization process is considered to be one of the most crucial factors that affects the performance of a biosensor. Recent reports have demonstrated that the presence of amine groups at the support surface can facilitate the effective immobilization of enzymes through covalent binding.^{8,39,45} Most of the commonly used HNT functionalization processes involve the utilization of dopamine³⁹ or APTES² to facilitate $-\text{NH}_2$ groups

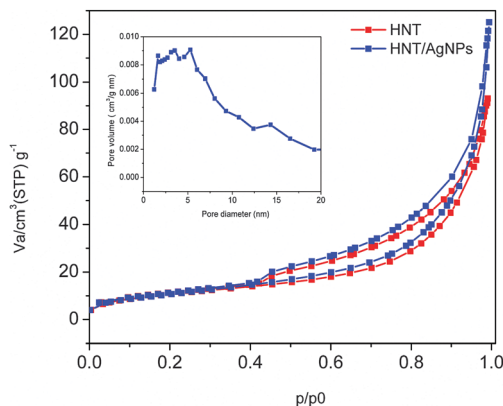


Fig. 4 Nitrogen adsorption–desorption isotherms of the pristine HNT and surface functionalized HNT/AgNPs. The inset shows the pore-size distribution in the HNT/AgNPs.

on their surfaces. In the present work we utilized APTES to further modify the HNT/AgNP surfaces for enzyme immobilization (Fig. 5a). APTES functionalized HNT/AgNP presents abundant $-\text{NH}_2$ groups on their surface, which reacts with glutaraldehyde (GA) to cross-link GOx enzymes on the surface. The covalent linkage formed between the $-\text{CHO}$ groups of GA is linked to the NH_2 groups of GOx *via* C–N bonds, while the other $-\text{CHO}$ groups interact with the NH_2 group of functionalized HNT/AgNP surfaces.^{12,45,46} Thereby, the covalent conjugation can be achieved, *i.e.* effective immobilization of the GOx takes place on the HNT/AgNP surface. The selective binding of GOx over HNT/AgNPs through amine groups and associated chemical changes have been confirmed by AFM and FT-IR spectroscopy, respectively. Fig. 5b shows representative FT-IR spectra of functionalized HNT/AgNPs and HNT/AgNP–GOx. The silane-modified HNT and HNT/AgNP hybrid composite exhibit characteristic transmittance bands.³⁸ After immobilization of GOx over HNT/AgNPs, peaks appeared at 1650 cm^{-1} and 1556 cm^{-1} , associated with the amide I (C=O stretching) and amide II (N–H bending) bonds, which indicates that the effective immobilization of GOx occurs *via* C–N bond formation between the GOx enzymes and the NH_2 terminated HNT/AgNP surfaces. These observations are in good agreement with previous reports on the covalent immobilization of GOx using GA as a bifunctional linker.^{12,45} Further investigation by AFM was used to elucidate the binding efficiency of the GOx over the HNT/AgNP surface (Fig. 5c). The AFM image clearly shows the effective binding of the GOx with the surface of the composite. Despite some agglomeration, majority of the GOx molecules are well attached to the composite surface, indicating good binding efficiency. The line profile analysis of a single surface-bound GOx indicates the height of individual GOx to be $\sim 15 \text{ nm}$ (Fig. 5d), which corresponds well with previous reports.^{10,33} The effective binding of GOx through AgNPs also makes the AgNPs to serve as electrical connectors to wiring the FAD-center of GOx and the electrode surface. Consequently, upon addition of glucose it reacts with the deeply buried FAD co-factor unit of the GOx and liberates two electrons by enzymatic reaction. The generated electrons were rapidly transferred to the electrode surface, significantly enhancing the sensitivity of glucose detection.^{14,47}

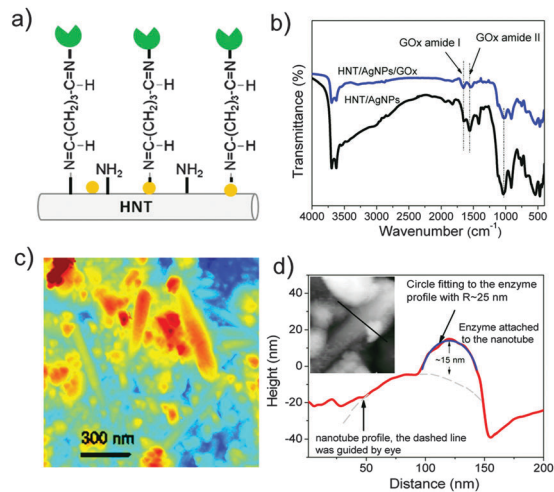


Fig. 5 (a) Schematic illustration of covalent linkage of GOx enzymes on HNT/AgNP surfaces using GA as a bifunctional linker; (b) FTIR spectra of HNT/AgNPs and the HNT/AgNPs/GOx; (c) a typical AFM topographical image and (d) cross-sectional analysis of the HNT/AgNPs/GOx, respectively. The inset in (d) shows the magnified image of the immobilized GOx on the HNT/AgNP surface.

Electrochemical characterization of DET and amperometric detection of glucose

To demonstrate the effective immobilization and wiring of GOx enzymes onto the electrode, we fabricated GOx immobilized HNT/AgNP composites incorporated in glassy carbon electrodes (GCEs), and tested their DET characteristics by amperometric detection of glucose using cyclic voltammetry (CV). For comparison, CVs were performed for the bare GCE, HNT/AgNPs-GCE, and HNT/AgNPs/GOx-GCE electrodes in N₂-saturated 0.1 M phosphate buffered saline (PBS, pH 7.4) at a scan rate of 50 mV s⁻¹. The respective CV plots are shown in the ESI,† Fig. S3. The CVs of the bare GCE and HNT/AgNP-GCE electrodes did not show any peaks in the measured potential range. However, the HNT/AgNP/GOx-GCE electrode revealed two well-defined redox peaks at the cathodic peak potential (E_{pc}) of -0.49 V and anodic peak potential (E_{pa}) of -0.42 V. The observed redox peaks are assigned to the standard oxidation and reduction potential of FAD/FADH₂ of GOx, which has a formal potential of -0.46 V vs. Ag/AgCl at pH 7.9 (FAD and FADH₂ are the oxidized and reduced forms of flavin adenine dinucleotide).⁴⁸

To study the electrochemical detection of glucose, CV measurements were carried out in O₂-saturated 0.1 M PBS (pH 7.4) at a scan rate of 50 mV s⁻¹, in the presence of glucose at different concentrations. Fig. 6 shows the cyclic voltammetry and respective calibration plot corresponding to the electrocatalytic reduction at a covalently immobilized HNT/AgNP/GOx enzyme electrode upon successive addition of glucose in electrolyte solution. The glucose sensing mechanism of a GOx functionalized HNT/AgNP modified enzyme electrode is based on the catalytic oxidation of glucose to D-gluconolactone and hydrogen peroxide (H₂O₂) via enzymatic reaction.⁴⁹ The sensitivity of the glucose biosensor can be evaluated by the amount of generated H₂O₂ from the enzymatic reaction. The AgNPs on the HNT surface act as efficient catalysts

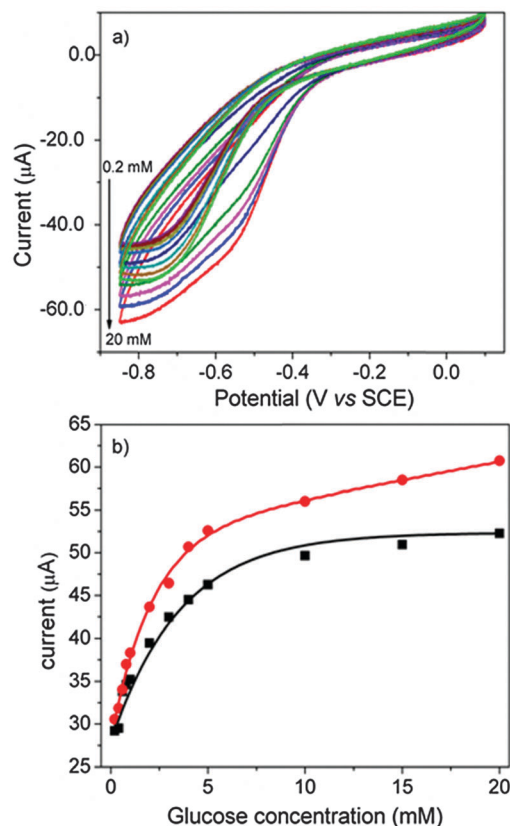


Fig. 6 (a) Cyclic voltammograms of the HNT/AgNPs/GOx-GCE in 0.1 M PBS (pH 7.4) with successive addition of glucose (0.1 to 20 mM); (b) comparative calibration plots of the covalently immobilized HNT/AgNPs/GOx enzyme electrode (in red) and unfunctionalized HNT/AgNPs/GOx-GCE electrode (in black) for the measured interval of glucose concentrations.

and also wire the FAD-cofactor of the GOx through covalent linkage, thus significantly enhancing the direct charge transport of the biosensor.⁵⁰ As seen in Fig. 6a, the reduction current gradually increases upon the addition of glucose in the electrolyte, exhibiting linear variation between 0.2 and 6 mM, and saturation beyond 6 mM. The calibration plot of the peak current vs. glucose concentration shows hyperbolic dependence (Fig. 6b). The sensitivities for glucose sensing for the modified and unmodified HNT/AgNPs/GOx electrodes were estimated to be 3.48 and 5.2 μA mM⁻¹ cm⁻², respectively. The observed variation in sensitivity upon covalent immobilization of GOx on the HNT/AgNP composite implies about a 50% increase. As noticed from the comparison presented in Table 1, the glucose detection sensitivity of our covalently immobilized HNT/AgNP/GOx enzyme electrodes is substantially higher than the sensitivities reported for other GOx immobilized electrode materials.

The results obtained in the present investigation demonstrate a pronounced enhancement in the sensitivity of the electrically contacted HNT/AgNP/GOx electrode for glucose sensing for a wide range of concentrations. The linear variation of reduction current with glucose concentration indicates the establishment of direct electrical contact between the FAD center of the GOx and the electrode surface through covalent bonding. The AgNPs play a key role by serving as a bridge to

Table 1 Comparison of analytical performance of different modified electrodes reported in the literature

Modified electrodes	Sensitivity ($\mu\text{A cm}^{-2} \text{mM}^{-1}$)	Linear range (mM)	Ref.
PMMA/diamond/GOx	0.006	0–3	8
DIM/Au25/GOx	0.21	1–6	51
CNT/GOx	0.47	1–30	52
CS/GOx	4.21	0.083–182	53
CS/Fe ₃ O ₄ NPs/GOx	1.2	0.01–0.027	54
AuNPs/TNT/GOx	5.1	0.01–1.2	55
BMIM/ γ -Fe ₂ O ₃ /GOx	0.045	0–1.5	56
GR/CNT/ZnONPs/GOx	5.36	0.01–6.5	57
HNT/AgNPs/GOx	5.2	0.2–6	This work

electrically wire the enzyme as well as a good electrocatalyst for the reduction of enzymatically produced H₂O₂. The observed results are consistent with the nanoparticle-mediated DET mechanism reported earlier.^{47,58} The strategy demonstrated here can be extended for other types of nanoparticles for the effective immobilization and enhanced charge transfer between redox enzymes and the electrode surface, opening up new possibilities for designing low-cost enzymatic biosensors.

Conclusions

In summary, we have demonstrated a facile and efficient method for fabricating HNT/AgNP hybrid composites by chelation of Ag⁺ ions with a NH₂-modified HNT surface, and their subsequent *in situ* reduction. By functionalizing the HNT/AgNP surface with APTES, GOx enzyme could be successfully immobilized through covalent binding. Effective modification of the HNT surface by NH₂ groups and bonding of Ag nanoparticles with their surfaces could be verified through FT-IR spectroscopy, TEM, and XPS analysis. Electrodes fabricated with the HNT/AgNP/GOx modified GCE were used for the electrochemical detection of glucose. The GOx immobilized composite electrodes revealed a high electrocatalytic activity for glucose reduction and facilitated enhanced charge transport. The glucose detection sensitivity of the composite electrodes was as high as 5.1 $\mu\text{A mM}^{-1} \text{cm}^{-2}$, which is considerably higher than the glucose sensitivity of the electrode fabricated by the non-functionalized HNT/AgNP surface. The enhanced sensitivity of GOx immobilized HNT/AgNP electrodes is the result of better immobilization of GOx and electrical wiring of FAD-centers to the electrode surface, and hence an improved direct charge transfer between GOx enzyme and the electrode surface. Owing to unique features such as high surface area, adequate inner diameter (comparable to the dimension of biomolecules), and good biocompatibility, HNTs are excellent supports for enzyme immobilization. Furthermore, the high electrical conductivity of AgNPs catalyzes the enzymatically liberated H₂O₂ and enables rapid charge transport to the electrode surface. Thus, the combined advantages of these two parameters make the HNT/AgNP hybrid composite a potential platform for efficient glucose sensing. Moreover, the use of amine modified HNT/AgNP hybrid composites for the site-specific immobilization of enzymes embraces the “green chemistry” principles that

promise a facile and low-cost strategy for effective immobilization and electrical wiring of biomolecules for the design of high-performance biosensors.

Acknowledgements

This work was supported by the DGAPA-UNAM post-doctoral fellowship. The authors are grateful to J. A. Munoz-Salas for assistance with the construction of the GCE electrodes, Ma. Lourdes Palma Tirado (Campus UNAM Juriquilla, Qro), for TEM measurements.

Notes and references

- 1 A. S. Bommarius and M. F. Paye, *Chem. Soc. Rev.*, 2013, **42**, 6534.
- 2 D. N. Tran and K. J. Balkus, *ACS Catal.*, 2011, **1**, 956.
- 3 J. Kim, H. Jia and P. Wang, *Biotechnol. Adv.*, 2006, **24**, 296.
- 4 K. E. Sapsford, W. R. Algar, L. Berti, K. B. Gemmill, B. J. Casey, E. Oh, M. H. Stewart and I. L. Medintz, *Chem. Rev.*, 2013, **113**, 1904.
- 5 T. Nöll and G. Nöll, *Chem. Soc. Rev.*, 2011, **40**, 3564.
- 6 A. Zebda, C. Gondran, A. Le Goff, M. Holzinger, P. Cinquin and S. Cosnier, *Nat. Commun.*, 2011, **2**, 1.
- 7 J. T. Holland, C. Lau, S. Brozik, P. Atanassov and S. Banta, *J. Am. Chem. Soc.*, 2011, **133**, 19262.
- 8 A. A. Reitingner, N. A. Hutter, A. Donner, M. Steenackers, O. A. Williams, M. Stutzmann, R. Jordan and J. A. Garrido, *Adv. Funct. Mater.*, 2013, **23**, 2979.
- 9 A. Trifonov, K. Herkendell, R. Tel-Vered, O. Yehezkeili, M. Woerner and I. Willner, *ACS Nano*, 2013, **7**, 11358.
- 10 M. Frascioni, A. Heyman, I. Medalsy, D. Porath, F. Mazzei and O. Shoseyov, *Langmuir*, 2011, **27**, 12606.
- 11 M. Radhakrishna and S. K. Kumar, *Langmuir*, 2014, **30**, 3507.
- 12 J. Narang and C. S. Pundir, *Int. J. Biol. Macromol.*, 2011, **49**, 707.
- 13 L. Li, Y. Shi, L. Pan, Y. Shi and G. Yu, *J. Mater. Chem. B*, 2015, **3**, 2920.
- 14 J. Lee, H. Ahn, I. Choi, M. Boese and M. J. Park, *Macromolecules*, 2012, **45**, 3121.
- 15 C. R. Parthasarathy and R. V. Martin, *Nature*, 1994, **369**, 298.
- 16 H. R. Luckarift, J. C. Spain, R. R. Naik and M. O. Stone, *Nat. Biotechnol.*, 2004, **22**, 211.
- 17 S. Patra, T. Hidalgo-Crespo, A. Permyakova, C. Sicard, C. Serre, A. Chausse, N. Steunou and L. Legrand, *J. Mater. Chem. B*, 2015, **3**, 8983.
- 18 X. Wu, J. Ge, C. Yang, M. Hou and Z. Liu, *Chem. Commun.*, 2015, **51**, 13408.
- 19 J. Zhang, J. Zhang, F. Zhang, H. Yang, X. Huang, H. Liu and S. Guo, *Langmuir*, 2010, **26**, 6083.
- 20 M. E. G. Lyons and G. P. Keeley, *Chem. Commun.*, 2008, 2529.
- 21 V. Scognamiglio, *Biosens. Bioelectron.*, 2013, **47**, 12.
- 22 S. Das and S. Jana, *Dalton Trans.*, 2015, **44**, 8906.

- 23 Y. Lvov, A. Aerov and R. Fakhrullin, *Adv. Colloid Interface Sci.*, 2014, **207**, 189.
- 24 P. Yuan, P. D. Southon, Z. Liu and C. J. Kepert, *Nanotechnology*, 2012, **23**, 375705.
- 25 C. Zhang, S. Luo and W. Chen, *Talanta*, 2013, **113**, 142.
- 26 B. Zhang, Y. Xing, Z. Li, H. Zhou, Q. Mu and B. Yan, *Nano Lett.*, 2009, **9**, 2280.
- 27 Y. Zhang, A. Tang, H. Yang and J. Ouyang, *Appl. Clay Sci.*, 2015, **119**, 8.
- 28 Y. Zhang, X. He, J. Ouyang and H. Yang, *Sci. Rep.*, 2013, **3**, 2948.
- 29 D. Brondani, C. W. Scheeren, J. Dupont and I. C. Vieira, *Sens. Actuators, B*, 2009, **140**, 252.
- 30 J. Wu and L. Yin, *ACS Appl. Mater. Interfaces*, 2011, **3**, 4354.
- 31 X. Jiang, J. Hu, A. M. Lieber, C. S. Jackan, J. C. Bi, L. A. Fitzgerald, B. R. Ringeisen and C. M. Lieber, *Nano Lett.*, 2014, **14**, 6737.
- 32 Y. Xiao, F. Patolsky, E. Katz, J. F. Hainfeld and I. Willner, *Science*, 2003, **299**, 1877.
- 33 F. Patolsky, Y. Weizmann and I. Willner, *Angew. Chem., Int. Ed.*, 2004, **43**, 2113.
- 34 J. S. Y. Chia, M. T. T. Tan, P. S. Khiew, J. K. Chin and C. W. Siong, *Sens. Actuators, B*, 2015, **210**, 558.
- 35 J. M. Goran, S. M. Mantilla and K. J. Stevenson, *Anal. Chem.*, 2013, **85**, 1571.
- 36 M. Ghosh, S. Maiti, S. Dutta, D. Das and P. K. Das, *Langmuir*, 2012, **28**, 1715.
- 37 P. Asuri, S. S. Bale, R. C. Pangule, D. a. Shah, R. S. Kane and J. S. Dordick, *Langmuir*, 2007, **23**, 12318.
- 38 M. L. Zou, M. L. Du, H. Zhu, C. S. Xu and Y. Q. Fu, *J. Phys. D: Appl. Phys.*, 2012, **45**, 325302.
- 39 C. Chao, J. Liu, J. Wang, Y. Zhang, B. Zhang, Y. Zhang, X. Xiang and R. Chen, *ACS Appl. Mater. Interfaces*, 2013, **5**, 10559.
- 40 S. Kumar-krishnan, E. Prokhorov, O. Arias de Fuentes, M. Ramirez, N. Bogdanchikova, I. C. Sanchez, J. D. Mota-Morales and G. Luna-Barcenas, *J. Mater. Chem. A*, 2015, **3**, 15869.
- 41 L. Yu, Y. Zhang, B. Zhang and J. Liu, *Sci. Rep.*, 2014, **4**, 1.
- 42 S. Kumar-Krishnan, E. Prokhorov, M. Hernández-Iturriaga, J. D. Mota-Morales, M. Vázquez-Lepe, Y. Kovalenko, I. C. Sanchez and G. Luna-Bárcenas, *Eur. Polym. J.*, 2015, **67**, 242.
- 43 E. Prokhorov, S. Kumar-Krishnan, G. Luna-Barcenas, M. Lepe and B. Campos, *Curr. Nanosci.*, 2015, **11**, 166.
- 44 P. Yao, S. Zhong and Z. Shen, *Int. J. Photoenergy*, 2015, 1.
- 45 L. Li, Y. Wang, L. Pan, Y. Shi, W. Cheng, Y. Shi and G. Yu, *Nano Lett.*, 2015, **15**, 1146.
- 46 L. Rodríguez-Lorenzo, R. de la Rica, R. a. Álvarez-Puebla, L. M. Liz-Marzán and M. M. Stevens, *Nat. Mater.*, 2012, **11**, 604.
- 47 O. Yehezkeli, R. Tel-Vered, S. Raichlin and I. Willner, *ACS Nano*, 2011, **5**, 2385.
- 48 P. Si, S. Ding, J. Yuan, X. W. Lou and D. H. Kim, *ACS Nano*, 2011, **5**, 7617.
- 49 R. A. S. Nascimento, R. E. Özel, W. H. Mak, M. Mulato, B. Singaram and N. Pourmand, *Nano Lett.*, 2016, **16**, 1194.
- 50 S. Kumar-Krishnan, S. Chakaravarthy, A. Hernandez-Rangel, E. Prokhorov, G. Luna-Bárcenas, R. Esparza and M. Meyyappan, *RSC Adv.*, 2016, **6**, 20102.
- 51 K. Kwak, S. S. Kumar, K. Pyo and D. Lee, *ACS Nano*, 2014, **8**, 671.
- 52 Y. Lin, F. Lu, Y. Tu and Z. Ren, *Nano Lett.*, 2004, **4**, 191.
- 53 C. Zhao, Y. Meng, C. Shao, L. Wan and K. Jiao, *Electroanalysis*, 2008, **20**, 520.
- 54 Z. R. Marand, N. Shahtahmasebi, M. R. Housaindokht, G. H. Rounaghi and I. Razavipanah, *Electroanalysis*, 2014, **26**, 840.
- 55 R. Zhao, X. Liu, J. Zhang, J. Zhu and D. K. Y. Wong, *Electrochim. Acta*, 2015, **163**, 64.
- 56 D. Baratella, M. Magro, G. Sinigaglia, R. Zboril, G. Salviulo and F. Vianello, *Biosens. Bioelectron.*, 2013, **45**, 13.
- 57 K.-Y. Hwa and B. Subramani, *Biosens. Bioelectron.*, 2014, **62**, 127.
- 58 S. Su, Y. He, S. Song, D. Li, L. Wang, C. Fan and S.-T. Lee, *Nanoscale*, 2010, **2**, 1704.